EUROFUSION WPJET1-CP(16) 15164

C Giroud et al.

Progress in understanding the role of low-Z impurity in the confinement of JET-ILW and in JET-C plasmas

Preprint of Paper to be submitted for publication in
Proceedings of 26th IAEA Fusion Energy Conference

This work has been carried out within the framework of the EUROfusion Consortium and has received funding from the Euratom research and training programme 2014-2018 under grant agreement No 633053. The views and opinions expressed herein do not necessarily reflect those of the European Commission.

Progress in understanding the role of low-Z impurity in the confinement in JET-ILW and in JET-C plasmas

C. Giroud[1], N. Aiba[2], S. Brezinsek[3], A. Chankin[4], E. Delabie[5], L. Frassinetti[6], I. Lupelli[1], D. Moulton[1], J. Simpson[1], P. Drewelow[6], A. Field[1], J. Hillesheim[1], A. Huber[3], M. Leyland[8], B. Lomanoski[1], S. Menmuir[1], S. Pamela[1], S. Saarelma[1], S. Wiesen[3], C. F. Maggi[1] and H. Urano[2] and JET Contributors*

EUROfusion Consortium, JET, Culham Science Centre, Abingdon, OX14 3DB, UK
[1] Culham Centre for Fusion Energy, Culham Science Centre, Abingdon OX14 3DB, UK
[2] National Institutes for Quantum and Radiological Science and Technology, Rokkasho, Aomori 039-3212, Japan.
[3] Forschungszentrum Jülich GmbH, Institut für Energie- und Klimaforschung – Plasmaphysik, Partner of the Trilateral Euregio Cluster (TEC), 52425 Jülich, Germany
[4] Max-Planck-Institut für Plasmaphysik, D-85748 Garching, Germany
[5] Oak Ridge National Laboratory, Oak Ridge, TN 37831-6169, Tennessee, USA
[6] Department of Physics, SCI, KTH, SE-10691 Stockholm, Sweden
[7] Max-Planck-Institut für Plasmaphysik, Teilinstitut Greifswald, D-17491 Greifswald, Germany
[8] University of York, Heslington, York YO10 5DD, UK
* See the Appendix of F. Romanelli et al., Proc. 25th IAEA FEC 2014, St Petersburg, Russia
e-mail: carine.giroud@ccfe.ac.uk

The pedestal confinement has significantly decreased in JET with its metallic ITER-like wall with reference to the carbon wall phase of JET (JET-C). In particular, a reduction in pedestal temperature is observed in all scenarios regardless of the level of D-gas injection or value of β_N [1-3]. At low gas injection, excessive W radiation is not always the cause for this reduction. Unraveling the mechanism(s) that, in the absence of carbon in the plasma composition and/or as wall material, leads to a decrease in pedestal temperature is critical in predicting the pedestal pressure in ITER. This mechanism(s) is most likely related to the observed increase in pedestal temperature with nitrogen (N) injection in JET-ILW[4], and should also explain the lack of pedestal pressure improvement with neon (Ne) injection[5]. This paper makes a synthesis of experimental observations made with extrinsic impurity injection since the first JET-ILW campaign in high-δ plasmas and reviews our current understanding of the role of low-Z impurity on the pedestal pressure highlighting the role of two mechanisms.

1. Difference in pedestal conditions and structure in high-δ JET-C and JET-ILW

In the JET-ILW 2.5MA/2.75T high-δ plasmas at $n_{ped}/n_{GW}>0.7$ with a inner and outer strike on the vertical and horizontal inner and outer target respectively (V/H), discharges most comparable with JET-C, the pedestal pressure has reduced by 40% with a decrease in pedestal

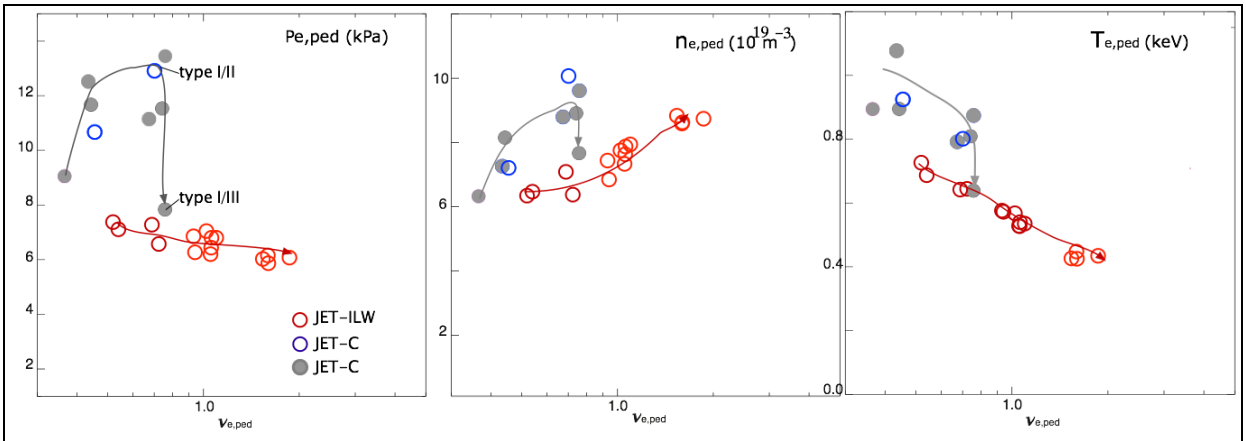

Fig. 1:pre-ELM electron pressure, temperature and density for high-δ unseeded JET-ILW (red), and JET-C (blue and grey) plasmas. Grey symbols indicates shots with vignetted HRTS measurements uncorrected, less reliable than data obtained in following campaign with improved HTS (blue point). Grey and red lines indicate an increasing D-gas rate

temperature from 0.9keV to 0.5keV with the change of wall, as shown in fig. 1 [6]. A comparison of the pre-elm pedestal pressure, temperature and density in JET-ILW and JET-C counterparts for a similar range of D-gas rate versus electron pedestal collisionality with similar input power 14-16 MW clearly highlights that similar range of density can be reached in JET-ILW but not at the same pedestal temperature. Added to this figure are the JET-C discharges from Ref. 7 in grey symbol for which the HRTS measurements could not be corrected for vignetting, and did not have as good an edge spatial resolution as for the following JET-C campaign (blue points, fig. 1). A comparison of the general trends of the pedestal structure with the higher HRTS resolved JET-C dataset (blue points) is however informative in these discharges which can no longer be repeated, in particular for the trend in the position of the peaked pressure gradient.

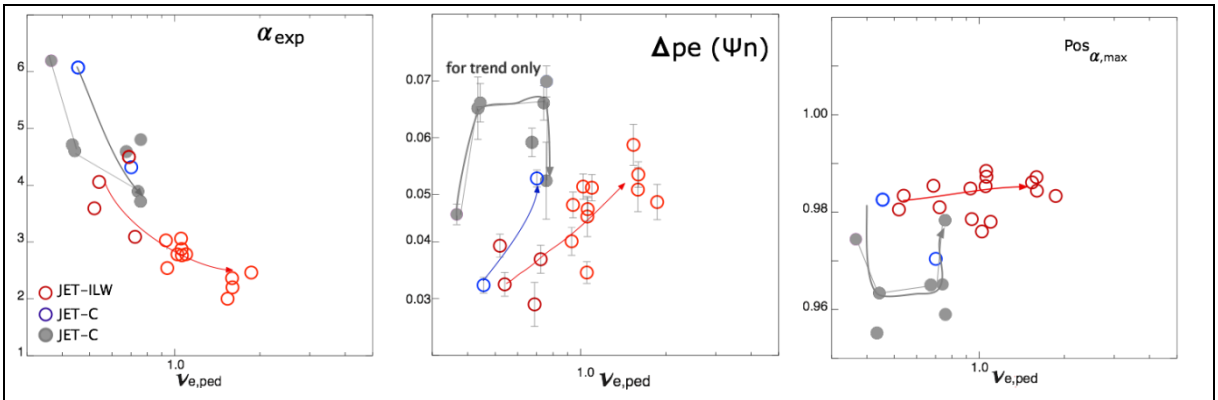

Fig. 2: pedestal peaked pressure gradient, pressure width and position of peaked pressure gradient in Ψn for JET-C and JET-ILW. For grey points, the pressure width shown for grey points only to indicate the trend in D-gas scan, values should be ignored. Legends as in Fig. 1

The pedestal structure of the JET-ILW and JET-C high-δ discharges, see fig. 2. The main difference in terms of pedestal structure is really at high collisionality (ν^*_e=0.7) where

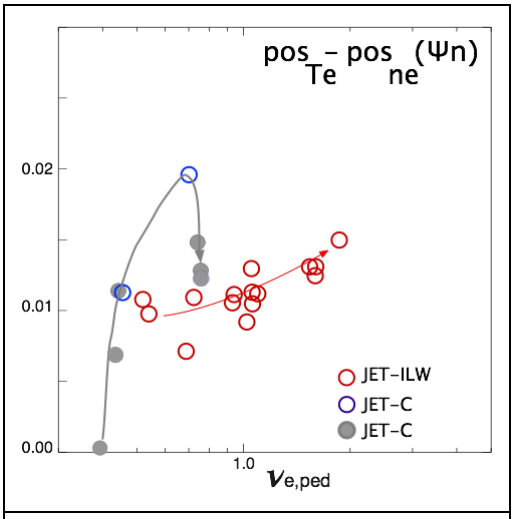

Fig.3 : Difference in position in ψ_n of electron temperature minus the electorn density. Legends as in Fig. 1

the same peaked pressure value of α_{exp}, and pedestal pressure width cannot be achieved (ignoring values of grey points). On the other hand, at low collisionality (ν^*_e=0.5) the pressure width can be matched but α_{exp} remains low at about 4 instead of 6. This region of low collisionality for the 2.5MA high-δ plasmas is however operationally difficult due to excessive plasma radiation due high W content. In fact, these high-δ plasmas in the collisionality range of 0.5-0.6 were not easily reproducible.

A closer look at the pedestal structure of the JET-C discharges (grey and blue points) indicate that the position of α_{max} moves inwards from 0.98 to 0.97 at high collisionality obtained with increased D-gas rate (conditions for the type-I/II ELMs), which is stabilising for the pedestal, with a relative shift between the position of the electron density and temperature pedestal increasing from 0.01 to 0.02,see Fig. 3, which should lower the bootstrap current and be more destabilising for the pedestal [8]. The position of α_{exp} is calculated with the assumption $T_{e,sep}$ equal a 100eV. In contrast, Fig. 2 highlights that the position of α_{exp} in JET-ILW at high collisionality is closer to the separatrix and more destabilising but a density and temperature pedestal closer to one another than in JET-C, see Fig. 3. As the D-gas rate increase, the position of α_{exp} barely increased and the relative position of pedestal temperature and density barely increases from 0.01 to 0.015 for collisionality 0.5 to 2. A new analysis of the older JET-C (grey points) dataset indicates that as the D-gas rate is increased the position of α_{exp} moves inwards and then outwards back to its original position when the pedestal is close to a transition to type-III ELM regime with similarly an increase and then decrease in the relative shift between electron density and temperature profile. A parallel can be drawn with the effect of N seeding in JET-ILW as will be seen in section 3.

These reference JET-C plasmas combined a wide pedestal and operation point that access the corner of the Peeling-Ballooning (PB) diagram [9], with pressure limited by intermediate n-numbers (n=5-20), whereas these JET-ILW unseeded plasmas have lower pressure gradient limited by high n-number ≥ 70 (ballooning modes) [4]. The pedestal stability has clearly been affected by a change of wall. The re-introduction of low-Z impurity (N) almost recovers the thermal stored energy, pedestal pressure and pedestal temperature T_{ped} to

JET-C levels and with an operation point in the corner of PB diagram.

2. Pre-elm pedestal pressure recovery and pedestal structure with N-seeding

The recovery of the pre-elm pedestal pressure has already been well documented in the high-δ discharges with V/H divertor configuration[6]. Figure 4 shows the change in peaked pressure gradient α_{exp} and pedestal pressure width and position of α_{exp} with N seeding at high D-gas rate of 2.5-3x10^{22} el/s. After an initial recovery in the α_{exp} at relatively low N seeding rate,

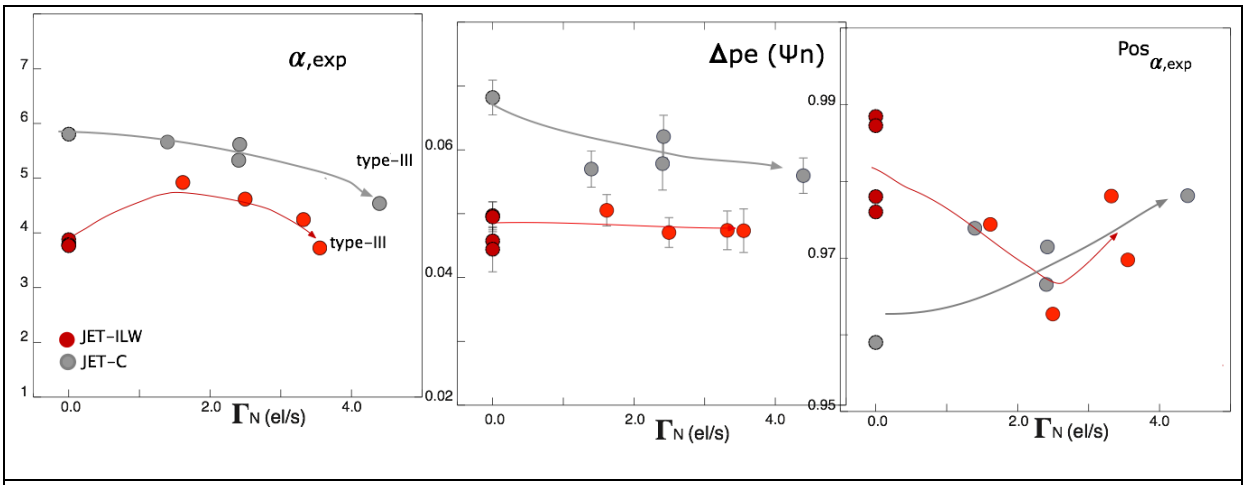

Figure 4: pedestal peaked pressure gradient, pressure width and position of peaked pressure gradient in Ψn for JET-C and JET-ILW as a function of N-seeding rate at high D-gas rate of 2.5-3x10^{22} el/s. . For grey points, the pressure width shown for grey points only to indicate the trend in N-gas scan, values should be ignored.

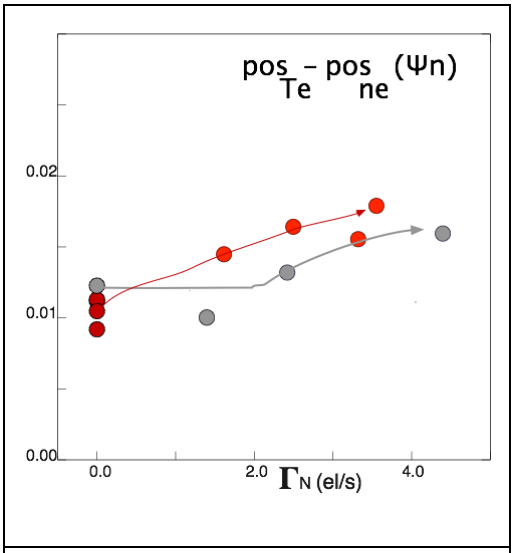

Fig.5 : Difference in position in ψ_n of electron temperature minus the electorn density as a function of N-gas rate . Legends as in Fig. 4

α_{exp} decreases with a similar trend to JET-C N seeded discharges. Depending on how wide is the pedestal for the unseeded discharges, the width increases with N seeding or stays constant. Similarly to the JET-C discharges with increased D-gas rate, the position of α_{exp} moves inwards with N-seeding in JET-ILW at low N-seeding (ΔZ_{eff} =0.3) rate down to 0.96 and moves back closer to the separatrix at higher seeding following a similar trend to what was observed in JET-C with N-seeding. In both cases, the relative shift of the electron density and temperature pedestal is increasing, see Fig 5. In JET, the improved pedestal stability in nitrogen seeding is caused by the pressure profile moving inward from the separatrix with impurity injection, even if the relative shift of the density and temperature profile increases, both well-resolved with high resolution

Thomson scattering. N-seeding in JET-ILW reproduces conditions for the position of α_{exp} of JET-C with D-gas as shown in previous section. In AUG, with full tungsten wall, seeding N (and CD_4) also leads to an increase in pedestal pressure, up to ~40% [10]. This rise is understood by a relative inward shift of the density profile attributed to a shrinking of a high density region on the high field side SOL (HFSHD) with N injection. In JET-ILW, a HFSHD is also observed and its reduction is seen both with N and Ne injection, but no increase in pedestal pressure with Ne is observed. In JET-ILW, the pedestal stability could also improve with a global shift of the profiles inwards due to the reduction of the separatrix temperature [8]. The reality seems more complex in JET-ILW with a mechanism(s) that is not solely linked to ideal linear PB stability since N-seeded plasmas in JET-ILW can be in type-III ELM regime and have a higher pedestal pressure than unseeded type-I ELMy H-mode [4].

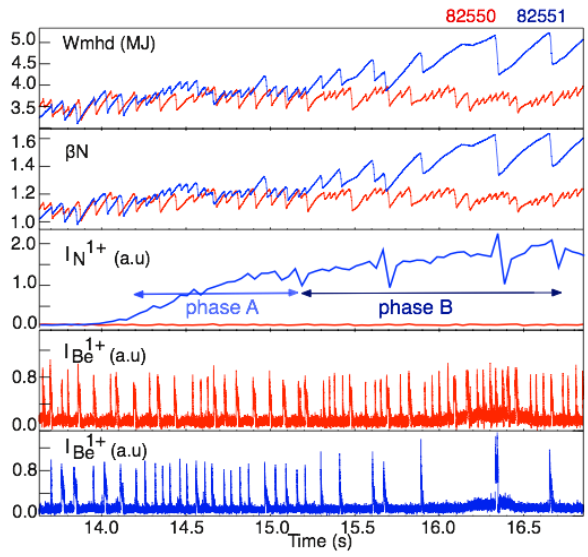

Fig. 6: Time dependence of reference high-™ plasma w/o N (82550) and with slow increase of N (82551), of stored energy, normalized pressure, nitrogen spectroscopic line intensity and ELM time trace.

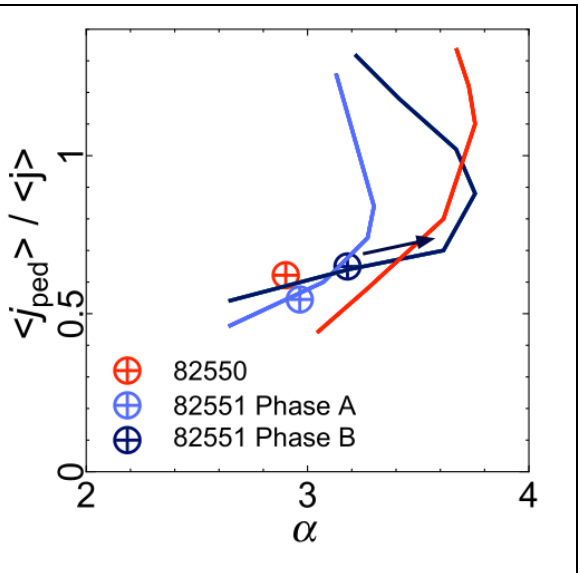

Fig. 7: Peeling Ballooning stability analysis for unseeded high-™ reference plasma (#82550) (stable) and seeded (#82551) during phase A (unstable n=60), when the average ELM losses reduced, and phase B (unstable n=36) when the pre-ELM pedestal pressure increases due to a tilt of stability boundary.

3. Pedestal evolution towards a enhanced pressure and identification of initial mechanism

The comparison of the operation point (OP) in the PB stability diagram has been puzzling. The stability boundary for the non-seeded and N-seeded cases are almost the same [8], but the experimental points are far from each other in the j-α diagram. The self consistent critical pressure in the two cases is almost the same, while the experimental pedestal height of the unseeded case is significantly higher. It was thought then that either something else

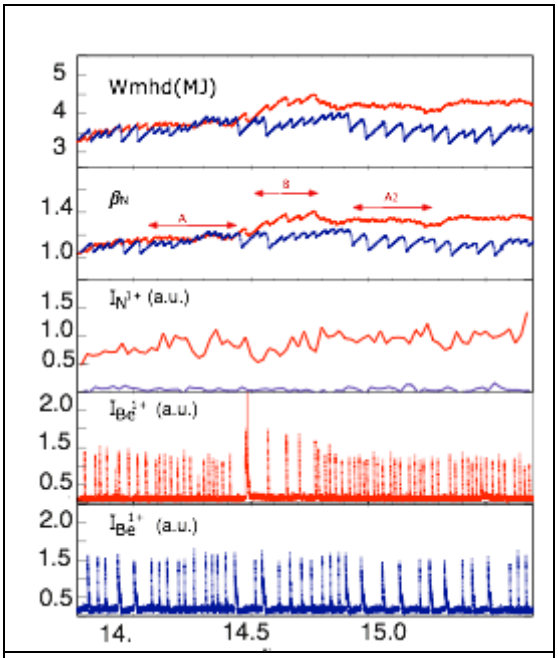

Fig. 8: time trace of 82554 (N-seeded) in red and 82546 (unseeded reference) in blue.

that the PB modes are limiting the unseeded pedestal to a lower pedestal pressure, or there is some mechanisms not captured by the bootstrap current formula used in this analysis that lowers the unseeded case pedestal current making it high-n ballooning mode limited at low values of α exp [8]

Below it is argued that N-seeding leads to an initial mechanism that changes the ELM energy losses, and often the ELM frequency, which raises modestly the average global β_N by 10% but allows in return a second mechanism to take place, provided certain pedestal conditions are fulfilled. The high-δ plasmas can then benefit, if in type-I ELM regime, from the virtuous cycle (2nd mechanism) of an increased Shafranov shift, higher pedestal pressure allowing increased core pressure [8]. An example of such a discharge is shot 82551 shown in figure 5. This discharge is different from the discharges described in section 2, with a well controlled N injection showing a fast rise and stationary conditions in the main plasma phase.

The shot 82551 has a slow rise in N content which makes the pedestal evolution easier to study. The rise of average global β_N by 10% can be seen in phase A with an operational point that comes closer to the stability boundary, and then in phase B to the operational point can "climb" towards the corner of the j-α diagram, see fig. 7. This would explain how N seeding re-establishes the improved pre-ELM pedestal pressure and therefore pedestal stability of high-δ plasmas with V/H divertor configuration. It would also clarify why in JET-ILW the recovery is dependent on plasma triangularity and on the chosen divertor configuration. The 1st mechanism which reduces the average ELM energy losses has to be identified but seems to be linked to the SOL/separatrix conditions. In the JET-ILW reference discharges, the ELM crash is longer (slow ELM) than in JET-C and characterized by two phases leading to larger ELM energy losses than in JET-C. With seeding, the second phase of slow ELM disappears[11] and the energy losses associated with slow ELMs decreases. In AUG, the slow ELMs tend to have pre-ELM divertor temperature higher than the short ELMs which suggest that the 2nd phase of the slow ELMs is related to the SOL temperature[11].

As the evolution of the pedestal is a highly dynamic process, it is difficult to point out to the reason for a difference in the pedestal evolution. However a dataset now exists with high-δ plasmas at similar collisionality unseeded, but resulting in different pre-elm pedestal pressure when impurity is seeded, either N, CD_4 or O. As shown in Fig. 9, conditions were obtained where N seeding does not manage to raise the pre-ELM pedestal pressure by more than 10%. Similar cases with CD_4 injection were also obtained with less than 10% increase in the pedestal pressure (89452) and another at lower D-gas fueling at $1.8x10^{22}$ el/s (89453, without accounting for D-injection due to the CD_4 itself) with a 30% increase in the pedestal pressure. Also added to this dataset, shown in fig. 9 is the evolution of discharge 82554. The pedestal makes a transition from phase A to phase B but cannot maintain the pedestal pressure increase and revert to phase A (or A1 Fig 8). Results are shown in fig, 9 for all the pulses mentioned.

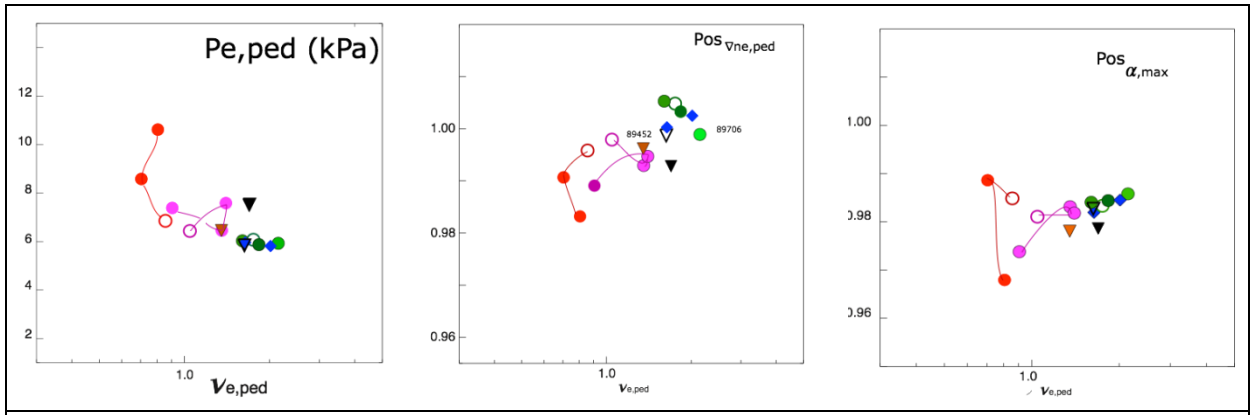

Fig 9: Pre-elm pedestal pressure and position and αexp calculated assuming Te eqiual to Ti. In red, shot 82550 unseeded (open), 82551 (filled, phase A linked to 82550, and phase B , red, filled). 82546 (open pink symbol) and 82554 (following from open pink symbol, phase A, phase B back to phase A2), 89454 (unseeded reference discharge for CD4 scan), 89452 (filled brown oran with CD4), 89453 (filled black, CD4), 89709 (open green symbol reference for high D-gas for N or O seeded scan) 89706 (light green),89704 (medium green), 89705 (dark green)., 89710,89711 (O seeded, blue points).

We have found that a crucial ingredient for the 1st mechanism to take place is the position of the gradient of density, as shown in fig 9. the pedestal pressure seems to be able to evolve further (2nd mechanism) if the resulting position of the α_{exp} is sufficiently shifted from the separatrix (ψ_n<0.97), as is the case for the 82551. In the case of the 89453 or 82554 with a position of α_{exp} (ψ_n>0.975), the conditions are not sufficient for 2nd mechanism to take place and the pedestal pressure improvement remains modest. The normalized pressure gradient using now both measured Te and Ti profiles (Ti_sep=2-3 Te,sep) for key discharges are shown in Fig 10. It illustrates further how the density gradient can influence the total pressure gradient. Figure 10 also shows pressure gradient for high-δ discharges with a divertor

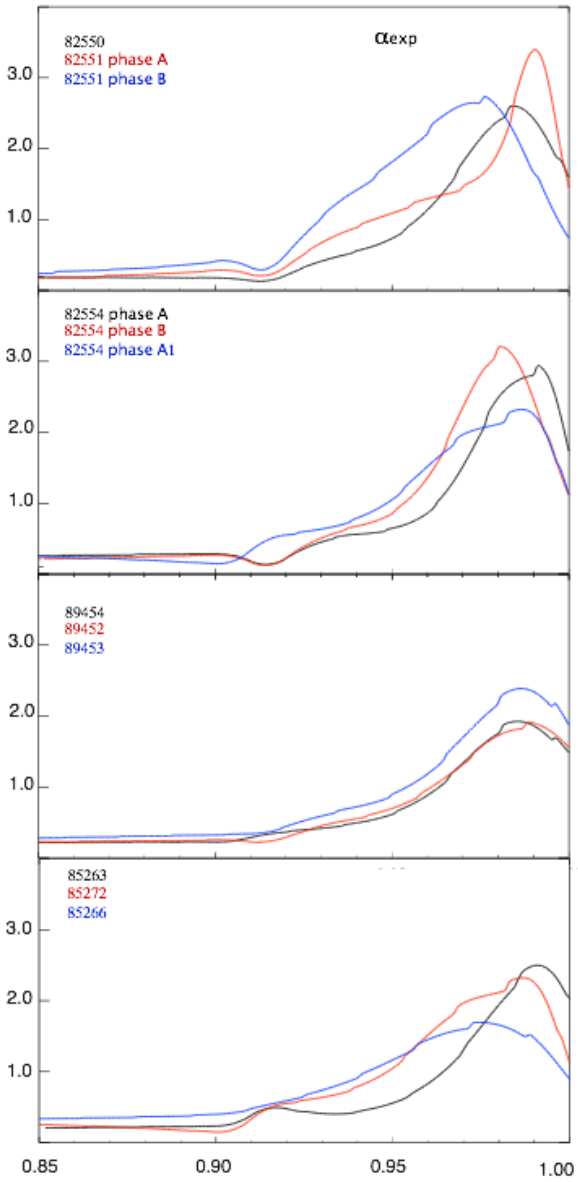

Fig. 10: Pedestal peaked pressure gradient calculated with both measured Ti and Te, for 82550, 82551, 82554, for the CD_4 series (89454,53 and 52) and for the high-d V/V plasma for 85263 (unseeded), for 85272,85266 (seeded)

configuration with vertical targets (V/V) with and without seeding where the increase in pre-elm pedestal pressure is about 15% [4] . These pressure gradients are very similar to phase-A1 of 82554 with similar results in increased pre-elm pedestal pressure. The high-δ plasmas with VV configuration cannot benefit for the 2nd mechanisms as their operational point lie removed from the PB boundary [4] The study of neon-seeded discharges will be part of a further investigation. Possible physics responsible for this 1st mechanism will be he aim of further work and discussed in the APS conference.

In conclusion, we have shown that the recovery of the pedestal pressure with N-seeding is the results of an evolution of pedestal due to a first mechanism still to be identified but linked to the position of the density gradient and the reduction of ELM energy losses. The second mechanism is taking place if the operational point of the pedestal is close to the PB boundary and result in an increased stability due to peaked pressure gradient positioned away from the separatrix. Demonstrating a physics understanding of the effect of low-Z impurity on the pedestal is critical in predicting the pedestal pressure in ITER and this paper aims to review our current understanding.

Acknowledgments

This work has been carried out within the framework of the EUROfusion Consortium and has receivedfunding from the Euratom Research and Training Programme 2014-2018 under grant agreement No 633053. The views and opinions expressed herein do not necessarily reflect those of the European Commission [1] Beurskens Nucl. Fusion **54** (2014) [2] Maggi Nucl. Fusion **55** (2015) [3] Nunes Plasma Phys. Control. Fusion **58** (2016) [4] Giroud Plasma Phys. Control. Fusion **57** (2015) [5] Giroud IAEA 2014[6] Giroud Nucl. Fusion **53** (2013) 113025[7] [8] Saarelma Phys. Plasmas 22, 056115 (2015) [9] Leyland Nucl. Fusion **53** (2015)[10] Dunne EPS 2015 [11] Dunne HMWS 2015 Frassinetti submitted Nucl. Fusion 2016